AIAA JOURNAL
Vol. 46, No. 10, October 2008

# Direct Reduction of Aero-Optical Aberrations by Large Structure Suppression Control in Turbulence

Aaron P. Freeman* and Haris J. Catrakis†
*University of California, Irvine, California 92697-3975*

DOI: 10.2514/1.36658

**Direct reduction of aero-optical aberrations incurred by a laser propagated through a refractive turbulent flow has been achieved by introducing plasma into the flow at various pulsing frequencies. The plasma is generated by a dielectric barrier discharge device which operates at elevated pressure to force flow near the separation point of a single-stream shear layer that is generated in a variable pressure wind-tunnel testing facility with $Re \sim 6 \times 10^6$ and $M_\infty \sim 0.9$. The levels of aero-optical aberrations present in the laser are determined by directly profiling the propagated laser using a high-resolution Shack–Hartmann wave front sensor with ~1000 microlenses. Reductions in the ensemble-averaged optical path difference root mean square of up to 27% were achieved. Whole-field shadowgraphs were recorded for various forcing frequencies and indicate that the observed aero-optical effects are the result of modifications in the level of organization of the large structures. Because the dominant contributions to the aberrations in unforced flows are caused by large-scale organized structures, our findings indicate that the mechanism by which the significant reduction is observed in the forced experiments is due to large-scale suppression of the turbulent structures directly effected by the pulsed plasma actuator. Conversely, increases in the aero-optical aberrations, which have also been observed at certain plasma pulsing frequencies, are the result of large-scale regularization of the structures within the turbulent shear layer. The presence of these large-scale suppression and regularization mechanisms is confirmed by the shadowgraphs at forced cases compared with the unforced case.**

## I. Introduction

AIRBORNE propagation of directed energy suffers consequences including reduced range, precision, and overall effectiveness, due to the interaction with varying refractive indices within the fluid medium through which it is propagated [1–3]. This is primarily due to the turbulent nature of aircraft-generated high-Reynolds-number separated flows that are typical in airborne applications. Namely, the flows associated with such applications tend to be turbulent and compressible. Accordingly, an important consideration for laser propagation in an optically active fluid medium is to account for various aberrations which are incurred along its propagation path, because the turbulent propagation medium of airborne lasers often exhibits multiscale and irregular variations in the refractive index [4,5]. The focus of this research is to characterize the aero-optical interaction between a turbulent flow and an aberrated-laser wave front profile for forced versus unforced cases, and to use the profiles to determine the level of control induced by a pulsed plasma actuator.

The field of aero-optics is concerned with the investigation of the interaction between propagated light and the fluid medium that it propagates through. Early work in aero-optics [1], as well as subsequent studies summarized in review articles, have illuminated several challenges in this field associated with both fundamental aspects as well as applications [6–8]. One goal of an aero-optical investigation is to physically relate the behavior of turbulence-generated refractive index fields to the structure of the turbulence-distorted optical wave fronts. Further understanding of the aero-optical properties within turbulent flowfields is a useful means of developing optical methods for probing large Reynolds number flows, especially in applications related to free-space laser communications, remote sensing of turbulence, or other uses of propagation of directed energy. The physical interaction that occurs between the fluid medium and the propagated optical wave fronts occurs across the refractive turbulent interface [9]. The refractive turbulent interfaces, at large Reynolds numbers, span wide ranges of scales and exhibit large levels of irregularity, thus rendering them difficult to theoretically characterize. However, the nature of aero-optics suggests optical diagnostics that allow for nonintrusive, high-speed direct profiling of turbulent flows. This research focuses on the ability to directly reduce the levels of aero-optical aberrations through periodic forcing of a turbulent shear layer.

Forced frequency control of a turbulent shear flow has been an active topic of research for several decades. Examples include the use of a pulsed jet that introduces fluid at the point of separation [10], miniature oscillating flaps [11], as well as applications which focus on manipulating fluid mixing in shear flows [12]. Previous research on flow control to explore aero-optical effects includes studies on acoustic forcing by Tsai and Christiansen [13] and Chew and Christiansen [14,15]. From the celebrated Kelvin–Helmholtz instability problem, it is well known that a thin shear layer, which behaves similar to a vortex sheet, is subject to various instabilities and associated growth rates based on fundamental frequencies which are present in the flow itself. Forcing of the flow by a prescribed frequency, often related to the passage frequency at the Kolmogorov scale or another fundamental length scale, is a means of encouraging the shear layer to behave a particular way by adding energy to the frequencies that actively contribute to the formation of large-scale, coherent, turbulent structures. In this research, where the primary focus is to directly reduce the levels of aero-optical aberrations present in a turbulence-aberrated optical wave front, it is important to keep in mind that the dominant contribution of aero-optical aberrations in the laser wave front are caused by the interaction with large organized turbulent structures [5,16]. Thus, the intended form of control over the shear layer is primarily to achieve the direct method of large-scale suppression (LSS) in an effort to produce desirable reductions of the associated effects on laser beam aberrations, as well as to assess the conceptual opposite of LSS, which can be termed large-scale regularization (LSR), which would

Presented as Paper 4008 at the 38th AIAA Plasmadynamics and Lasers Conference, Miami, FL, 25–28 June 2007; received 15 January 2008; revision received 22 June 2008; accepted for publication 28 June 2008. 

*Graduate Student, Mechanical and Aerospace Engineering; freemana@uci.edu. Member AIAA.

†Associate Professor, Mechanical and Aerospace Engineering; catrakis@uci.edu. Member AIAA.

be associated with undesirable increases of the aberrations. Though a detailed physical description of the mechanism that causes the LSS and LSR remains an open question, various explanations have been proposed that suggest the possibility of an acceleration in the energy cascade as the result of high-frequency forcing with piezoelectric actuators [11], as well as the possibility of a deceleration in the energy cascade resulting from high-frequency forcing using resonance tubes [17]. The present study is focused on forcing of the separated shear layer, also known as the single-stream shear layer, which is a prototypical flow geometry for both turret-based and cavity-based airborne laser ports. Additionally, this research offers the novel feature of forcing by means of a plasma actuation device to directly reduce the laser aberrations.

In this research, a laser sheet is propagated through a turbulent shear flow that results in an aberrated optical wave front. The laser is profiled using a custom-built Shack–Hartmann wave front sensor, which is a high-resolution optical device capable of simultaneously measuring the intensity and phase of a collimated light source. From the recorded phase and intensity, the optical wave front can be reconstructed and compared with the unaberrated, or uniform, wave front. The experiment is conducted with forced and unforced conditions relating to the introduction of plasma into the flow. Forcing is realized through the introduction of pulsed plasma into the flow. The plasma in this research is generated from a dielectric barrier discharge device at a frequency of 50.0 kHz and pulsed at frequencies ranging between 1.0 and 25.0 kHz. The flow conditions for these experiments result in a freestream velocity of $U_\infty \sim 300$ m/s and an initial momentum thickness of $\theta \sim 1.0$ mm. The corresponding range of Strouhal numbers, defined as $St = F\theta/U_\infty$, based on the pulsing frequencies $F$, initial momentum thickness, and freestream velocity is $0.003 < St < 0.09$. The level of suppression or regularization of aero-optical aberrations, and therefore LSS or LSR of the turbulent structures within the flow, is determined by examining the root mean square of the optical path difference of the associated turbulence-aberrated laser wave front profiles. Previous research in this field has focused on the ability for flow control mechanisms to exhibit LSR of the turbulent flows, which effectively increases laser aberrations, and then use adaptive optics to compensate for the resulting changes [18]. Although this method seems to have been the first flow control approach at reducing laser beam aberrations, it focuses on LSR, which is an indirect means of achieving the desired result. The possibility of directly reducing the laser beam aberrations through LSS is a more practical, robust, and broadly applicable approach because LSR of turbulent flows, although conceivable for simple flow geometries, can become increasingly difficult for more complex flow configurations.

Section II of this article will discuss the design and implementation of the Shack–Hartmann wave front sensor used in this research, along with the physical aspects that can be determined from the recorded data, including aspects of the LSS and LSR that are associated with the use of the pulsed plasma actuator (PPA). Section III will discuss the relevant aspects of the dielectric barrier discharge pulsed plasma actuator that is used to forced the shear layer in this research. The results and conclusions are discussed in the final two sections.

## II. Shack–Hartmann Wave Front Sensor

As discussed, the Shack–Hartmann (SH) sensor is a high-resolution optical device which simultaneously measures the phase and intensity of a collimated light source. The ability of the SH sensor to profile laser aberrations that are incurred by variable refractive index fields has been demonstrated in applications related to heated flow, evaporation, and identification of large turbulent structures [19,20]. In this research, the light being profiled is a turbulence-aberrated laser wave front that has incurred aberrations due to propagation through a compressible separated turbulent shear layer. Previous research regarding the aero-optical effects of light propagated through a shear layer includes work by Tsai and Christiansen [13] and Chew and Christiansen [14,15], who conducted both numerical and experimental studies to explore aero-optical effects on shear layers, including the effects of acoustic forcing. The SH sensor is a combination of a microlens array and a charge-coupled device (CCD) camera which records the light focused onto it by the microlenses. As seen in Fig. 1, the microlenses are mounted at a distance of one focal length $f$ away from the CCD pixel array. The result of this is the ability of the CCD camera to record the intensity of the focused wave front, as well as the spot displacement compared with the uniform wave front profile.

The SH sensor used in this research was built from commercially available components. The microlens array has 1024 positive (convex) refractive microcylinder lenses, each with a focal length of 10 mm at 532 nm and a pitch of 84 $\mu$m. The lenses are made of optical quality, UV-grade fused silica. The microlens array was built by Advanced Microoptics Systems in Saarbrücken, Germany. The CCD camera used in this research was the Piranha2 P2-80-12k40 model manufactured by Dalsa. The camera has a full resolution of 12,288 pixels, each with a size of 49 $\mu$m$^2$. The camera was operated through a LabView virtual interface that was facilitated by the National Instruments data acquisition card, NI-IMAQ PCIe-1429.

The pitch of the microlenses plays a distinct role in the ultimate resolution of the sensor itself. Because each of the microlenses contributes a discrete portion of the propagated laser wave front onto the CCD pixel array, more lenses will ultimately result in a higher-resolution representation of the propagated wave front. However, the microlenses must be larger than the pixels on the CCD camera to ensure that the resulting spot displacement can be accurately determined without ambiguity as to which microlens contributed a particular portion of light. Therefore, the ratio of the number of pixels to the number of microlenses, in addition to the focal length, are important quantities to consider to ensure appropriate data are recorded and will yield useful physical information. The pixel-to-microlens ratio used in this research, as determined from previous works in the design of wave front sensors [7], was ~12. The previously noted works demonstrated the choice of microlens diameter as a means of satisfying the required ratio. Alternatively, this research focused on the incorporation of a fixed quantity of microlenses, which then determined the diameter to be used with a particular CCD camera.

The particular CCD camera used in this research has 12,288 pixels in the 1-D array, with a sampling rate of 20 kHz. Each pixel has an area of 49 $\mu$m$^2$. The laser used in this research is a frequency-doubling Nd:YAG laser that generates light at 532 nm. The laser produced a 50 mJ pulse for approximately 5 ns at a rate of 10 Hz. Though the laser can produce light at a much lower frequency than the camera can capture data, it allowed for minimal efforts regarding the synchronization of the laser and the CCD camera.

Various physical quantities, which can be determined by directly profiling the optical wave front of a collimated light source, include

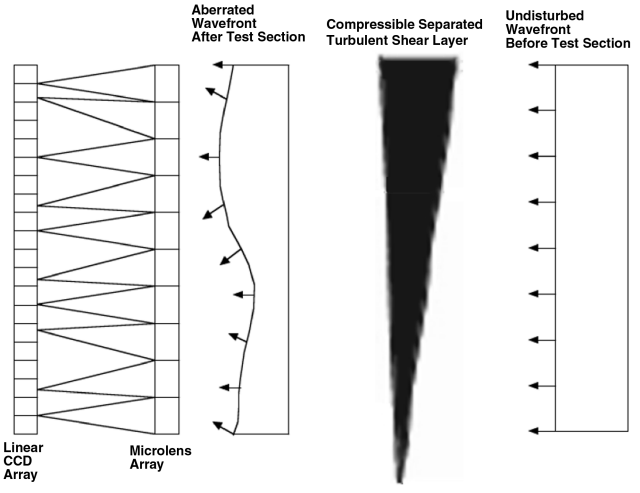


**Fig. 1 Schematic of the 1-D Shack–Hartmann microlens array and CCD sensor for profiling wave front aberrations resulting from forced and unforced compressible separated turbulent shear layers.**

the optical path length (OPL), optical path difference (OPD), and the root mean square of the OPD. The OPL is a function of the refractive index and the geometric distance that a ray of light travels. Because the refractive index of the compressible turbulent flows encountered in this research is not constant, the following mathematical equation is used to describe the OPL:

$$\mathrm{OPL}\,(\mathbf{x}, t) \equiv \int_{\mathrm{ray}} n(\ell, t)\,\mathrm{d}\ell \tag{1}$$

In Eq. (1), the physical distance along the beam propagation path for each ray of light is denoted as $\ell$. Because the OPL is related to the optical phase, or wave front propagation time, the wave fronts can be represented as isosurfaces of the OPL which correspond to $\mathrm{OPL}(\mathbf{x}, t) = \text{constant}$. A physical description of the OPL is that a ray of light, which travels a path of a given OPL, will arrive with the same phase shift as if it had traveled a path of equal physical length in vacuum.

The OPD represents the difference in OPL between two different propagated rays of light. In the case of a laser sheet, this quantity can be expressed as the difference between the OPL and the associated mean of that profile:

$$\mathrm{OPD}\,(\mathbf{x}, t) \equiv \mathrm{OPL}(\mathbf{x}, t) - \overline{\mathrm{OPL}(\mathbf{x}, t)} \tag{2}$$

For each experiment in this research, the OPD can be determined, which visually demonstrates how the turbulence generated aberrations in the propagating laser sheet. By direct comparison with the OPD profile of the unaberrated laser sheet, the interaction between the laser light and the turbulent fluid medium can be realized. Once the OPD of a particular laser sheet is known, the $\mathrm{OPD}_{\mathrm{rms}}$ can be computed directly. The $\mathrm{OPD}_{\mathrm{rms}}$ is a physical interpretation of the levels of aberrations within a particular OPD profile. This is one of the most relevant pieces of physical information determined by the SH sensor in this research because particular values of the $\mathrm{OPD}_{\mathrm{rms}}$ are used to compare the forced and unforced shear layers. In this research, because direct profiling of laser sheets is conducted, the resulting OPD is a profile. Mathematically, the $\mathrm{OPD}_{\mathrm{rms}}$ is found by taking the root mean square of the data which represent the OPD profile. Previous research in the same facility [21,22] with a different SH sensor found the $\mathrm{OPD}_{\mathrm{rms}}$ of the unforced shear layer to be 0.2 $\mu$m. This was verified for these sets of experiments with the new SH sensor.

The location of the centroid of each focal spot is determined using a reference wave front (i.e., with no flow). As noted, there are approximately 12 pixels onto which each of the microlenses projects a portion of the wave front. Thus, with the microlenses focused properly in front of the CCD pixel array, there is an intensified region, or bright spot, located once in every set of 12 pixels. An algorithm is implemented which identifies the location of the highest pixel intensity value for each set of 12 pixels. The location of the highest pixel intensity value within the span of the 12 pixels is recorded into an array which contains the data for the total number of wave fronts in each experiment.

The optical tilt is calculated using the values of the centroids of the reference image and the centroids of the images that were recorded with the turbulent flow present in the wind-tunnel test section. The optical tilt is determined by simply subtracting the centroid values in the array for the reference image from the centroid values in the array for the images with flow present. The resulting tilt values are related to the slope of the wave front and can be calculated through the following relationship:

$$\frac{\mathrm{d}W}{\mathrm{d}x} = -\tan\left(\frac{d}{f}\right) \approx -\frac{d}{f} \tag{3}$$

In the preceding equation, the value $f$ represents the focal length of the microlens array, $d$ represents the displacement of the centroids, and $W$ is the wave front phase. Because the array used in this research is one dimensional, the preceding equation only needs to be defined in the $x$ direction. The approximation shown in Eq. (3) is validated due to the large number of microlenses which have been incorporated as part of the SH sensor design. Once the local values of the slope of the wave front are known along its entire length, the wave front can be linearly reconstructed by integrating the local values of the wave front phase slope.

The error in the measurements taken by the SH sensor was quantified by calculating the $\mathrm{OPD}_{\mathrm{rms}}$ with no flow present in the wind tunnel. The standard deviation of the $\mathrm{OPD}_{\mathrm{rms}}$ values for profiles recorded for the no-flow case was calculated to determine a statistically repeatable value of the error. This value was calculated as $\pm 0.8\%$. In the forced-flow results reported next, this error is smaller than the standard deviation associated with the variations in the $\mathrm{OPD}_{\mathrm{rms}}$ for different realizations of forced flow at given forcing frequencies, which are shown in Table 1 and described in Sec. V.

## III. Pulsed Plasma Actuator

Plasma, used in this research to force the turbulent shear layer, is generated using a custom-built dielectric barrier discharge pulsed plasma actuator that can operate at atmospheric as well as elevated pressures. The present work builds on previous studies in the same facility that focused on the design and development of the electrical circuit necessary for the plasma actuator [23]. Frequency forcing of turbulent shear layers has been an active topic of research for several decades. In 1982, Oster and Wygnanski demonstrated that forced oscillations could cause changes in the shear layer growth rate and were even able to achieve resonant modes in the large structures depending on the amplitude [24], during which little or no pairing of the large structures was found to occur. In contrast, they also demonstrated that varying the frequency of the oscillation could encourage pairing. The work of Ho and Huerre in 1984 helped determine that the vortical structures found in a turbulent shear layer can be controlled using forced disturbances at the point of separation [25].

The incorporation of a plasma generation device as a flow control mechanism is novel in that it can be surface mounted, preventing unnecessary interaction between the flow and bluff bodies, such as flaps or slats, and it has no moving parts. Previous work in flow forcing using plasma actuation includes controlling structures within a von Kármán vortex street [26], comparison with physical flow-controlling flaps and slats [27], and control of flow separation over an airfoil [28]. Forcing is achieved by the fact that plasma, when introduced into a flow, induces an electrostatic body force on the surrounding fluid which is proportional to the net charge density:

$$\mathbf{F} = \rho_q \mathbf{E} = \frac{\epsilon_0}{\lambda_D^2}\phi\mathbf{E} \tag{4}$$

In the preceding equation, $\rho_q$ represents the net charge density which is defined by the ratio of the permittivity of free space and the square of the Debye length. The electric potential is $\phi$, and $\mathbf{E}$ is the electric field vector. Previous work in the control of both laminar and turbulent flow using a plasma actuator [29,30] demonstrated that both the displacement thickness $\delta^*$ and the momentum thickness $\theta$ are locally attenuated near the point where plasma is introduced into the flow, thus stabilizing the boundary layer near that location. This is caused by the body force shown in Eq. (4). Full descriptions of the local velocity fields for plasma generation into quiescent air, as well

**Table 1 Experimental results on the $\mathrm{OPD}_{\mathrm{rms}}$ values and percent changes for various flow control conditions; $F_{\mathrm{gen}}$ is the plasma generation frequency and $F_p$ is the plasma pulsing frequency**

| $F_{\mathrm{gen}}$, kHz | $F_p$, kHz | $\mathrm{OPD}_{\mathrm{rms}}$, $\mu$m | Total effect, % |
|---|---|---|---|
| —— | —— | 0.200 | —— |
| 50.0 | 1.0 | 0.234 | +16.9 |
| 50.0 | 5.0 | 0.145 | −27.5 |
| 50.0 | 10.0 | 0.192 | −4.0 |
| 50.0 | 12.5 | 0.157 | −21.7 |
| 50.0 | 25.0 | 0.204 | +2.41 |

as into a freestream velocity field, have been conducted in previous research [29].

The surface-mounted PPA is built into the flow facility such that it is the final stage of the wind tunnel and acts as the point of separation for the shear layer (see Fig. 2). The physical dimensions of the PPA, using the nomenclature from Fig. 3, are $L_{\mathrm{PPA}} = 0.01$ m, $h_{\mathrm{PPA}} = 0.002$ m, and $k_{\mathrm{PPA}} = 0.0015$ m. The spanwise length of the PPA $L_w$, which is also the width of the wind tunnel, is 0.3 m.

As noted previously, the dominant contributions to aero-optical aberrations are largely due to light propagation through large-scale turbulent structures [16]. Thus, the implementation of the PPA in this research is primarily to reduce or suppress the formation of such structures in the turbulent shear layer used in this research, to directly reduce aero-optical aberrations present in an optical wave front subsequent to its propagation through the shear layer. As seen in previous studies, the nature of the turbulent shear layer can be significantly altered by various external amplitude and frequency inputs [24,25].

A dielectric barrier discharge plasma actuation device consists of two parallel plates in an asymmetric configuration with a dielectric barrier between them (see Fig. 3). An ac current is applied between the two plates which effectively causes dissociation in the air molecules above the device. The generation of plasma occurs in two half-cycles, one in which the exposed electrode has a negative charge applied to it, allowing the insulated electrode to emit electrons. In the other half-cycle, the exposed electrode has a positive charge applied to it which attracts the electrons that were previously deposited on the dielectric. Previous research in this facility has demonstrated the ability for this plasma actuation device to generate a continuous and full plasma with ac currents from 10–100 kHz [23]. Figure 4 shows the various output voltages applied to the dielectric barrier discharge device as a function of input voltage for the plasma generation frequencies considered.

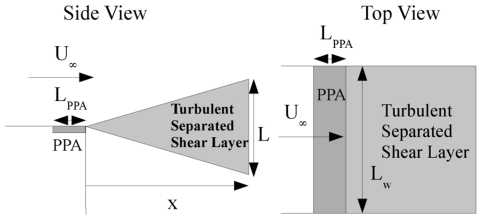


**Fig. 2 Schematic of the side and top views of the pulsed plasma actuator mounted inside of the flow facility.**

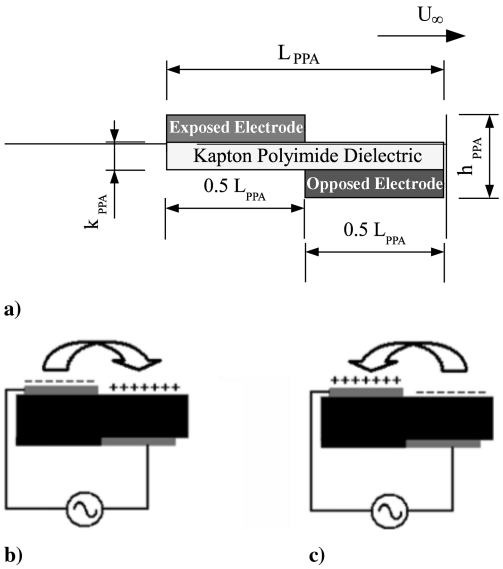


**Fig. 3 Plasma actuator: a) schematic of PPA, including various dimensions and physical location relative to freestream velocity; diagram showing b) negative cycle and c) positive cycle of the dielectric barrier discharge plasma actuator.**

For this research, plasma is generated inside a variable pressure wind-tunnel test section. Accordingly, the PPA must be able to generate plasma at the prescribed test section pressures. Increased pressure causes the generation of plasma to become more difficult. As the pressure increases, more molecules are present above the dielectric barrier discharge device, and thus more collisions occur between the electrons and the gas molecules, therefore requiring higher voltages to generate plasma fully along the length of the actuator. Once the voltages required to generate full plasma are known, the pulsing of the plasma on and off can be executed to control the formation of large turbulent structures within the shear layer.

This research studies the effects of the plasma actuator regarding the direct suppression or regularization of large turbulent structures within the turbulent shear layer. The plasma can be generated with a voltage signal at frequencies ranging from 20.0 to 80.0 kHz (see Fig. 4). For the Shack–Hartmann results shown here, the voltage signal frequency is set at 50.0 kHz, and pulsing in the form of an imposed on/off envelope is conducted at pulse frequencies ranging from 1.0 to 25.0 kHz. Although the range of pulsing frequencies is large, only certain generation-pulsing frequency combinations were achievable within the voltage range of the circuit used to operate the plasma actuator. At frequency combinations different than the ones reported in the results section, the plasma was not fully distributed along the length of the actuator. To achieve a full distribution of active plasma generation, higher voltages than could be generated with the current actuator setup would be required.

## IV. Experimental Facility and Procedure

The experiments for this research were conducted in the Turbulent Variable Pressure Facility (TVPF) at the University of California at Irvine (UC Irvine, Fig. 5). The TVPF is a turbulent flow testing facility that contains an assortment of optical equipment for advanced techniques in flow visualization and nonintrusive flow diagnostics through the use of lasers. The facility is adaptable and upgradable to accommodate future research in turbulence and aero-optics. This facility consists of a blowdown-type wind tunnel that is enclosed within a pressure vessel. The facility contains two primary "U"-stamp American Society of Mechanical Engineers rated pressure vessels, one that acts as the reservoir and the other to house the wind tunnel. The nonintrusive diagnostics of turbulent flows is facilitated by a 50 mJ, frequency-doubled Nd:YAG laser. A thorough description of this laser is provided in Sec. II.

High-pressure air from the reservoir tank is fed into the variable pressure tank, through the wind tunnel, encountering a set of flow straighteners along the way. Before entering the test section, the flow travels through a converging section. The nozzle is abruptly ended on one end with a sharp 90 deg corner. This enables a fixed and steady separation point and allows for the repeated generation of single-stream shear layers. Figure 6 shows a schematic of the wind-tunnel test section where the shear layer is formed. In the present research, each test used reservoir and test section pressures of 9.0 and 3.0 atm,

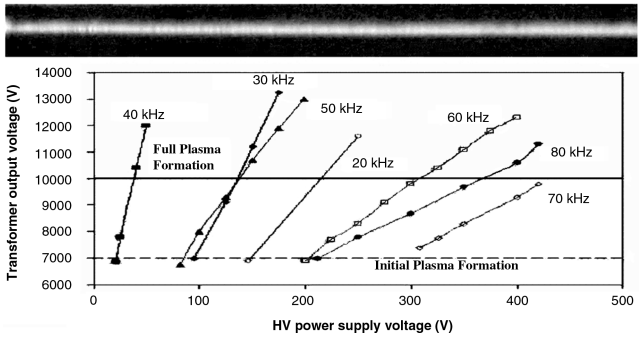


**Fig. 4 Top image shows a close-up photograph of the plasma optical emission showing full plasma formation across the entire 12-in. span of the actuator. Bottom plots shows high voltage output vs voltage input used to generate plasma at various generation frequencies.**

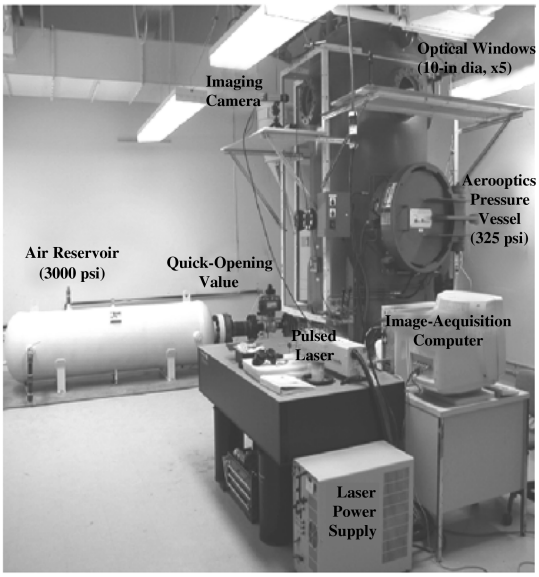


**Fig. 5 Photograph of the variable pressure turbulent flow facility at UC Irvine for high-resolution flow imaging and optical wave front measurements in forced and unforced flows at large Reynolds numbers with compressibility effects.**

respectively. The flow conditions inside the test section are $Re \sim 6 \times 10^6$ and $M_\infty \sim 0.9$. These testing conditions allow for the formation of a compressible separated turbulent shear layer.

For each test, the plasma is set to generate at a specific frequency, and pulse at a frequency that is an integer multiple of the generation frequency. This was done due to unsteady plasma formation that was found to occur at arbitrary pulsing frequencies. The laser and SH sensor are operated from the computer terminal and are timed to occur before the release of air into the wind tunnel. The data from the SH sensor initially need to be manually reduced to isolate the exact frame which captured the onset of turbulence, after which the reduction of data is fully automated.

## V. Results

The PPA and SH sensor were tested simultaneously to determine the aero-optical effects the plasma actuator had on the turbulent shear layer. In particular, the root mean square of the OPD profiles were calculated for the various forced versus unforced cases. Previous research in this facility has demonstrated the unforced shear layer results in an $\mathrm{OPD_{rms}}$ value of $\sim 0.2\ \mu$m. Accordingly, various increases or decreases in the value of the $\mathrm{OPD_{rms}}$ for the forced cases will correspond to a respective suppression or regularization in the distribution of large turbulent structures within the shear layer (LSS and LSR). Figure 7 shows examples of shadowgraph images of the unforced shear layer as well as the shear layer forced with the PPA. The bottom two images in Fig. 7 show examples of LSS and LSR, respectively.

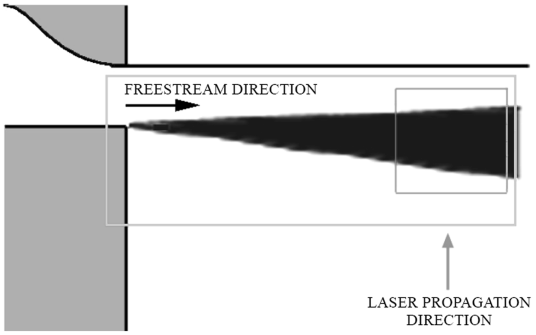


**Fig. 6 Schematic of the wind-tunnel test section where the turbulent shear layer is formed over a sharp 90 deg corner. Actual flow through the wind tunnel is oriented vertically.**

The OPD profiles for the forced and unforced cases can be seen in Fig. 8. These figures demonstrate the OPD profiles for the unforced shear layer, as well as the shear layer, which have been forced by the introduction of plasma generated at 50.0 kHz and pulsed at various incremental frequencies between 1.0 an 25.0 kHz.

Both the unforced experiments as well as those with forcing were repeated, as highlighted in Fig. 8, to yield an ensemble average of the $\mathrm{OPD_{rms}}$ values calculated for each run. Table 1 shows the results of the average value, based on 10 experiments each, of the $\mathrm{OPD_{rms}}$ for the various pulsing frequencies tested in this research.

In addition to the calculation of the $\mathrm{OPD_{rms}}$ values for the forced and unforced experiments, the spectra of particular OPD profiles was calculated to determine the ranges of scales which were recorded by the SH sensor. Figure 9 shows graphs of the resulting spectra in addition to a line which represents a power law scaling of $k^{-5/3}$, which can be found in traditional turbulence data of the velocity. These spectra results are calculated from the scalar refractive index fields and verify that the SH sensor is recording data related to the inertial ranges of scales found in turbulence. In particular,

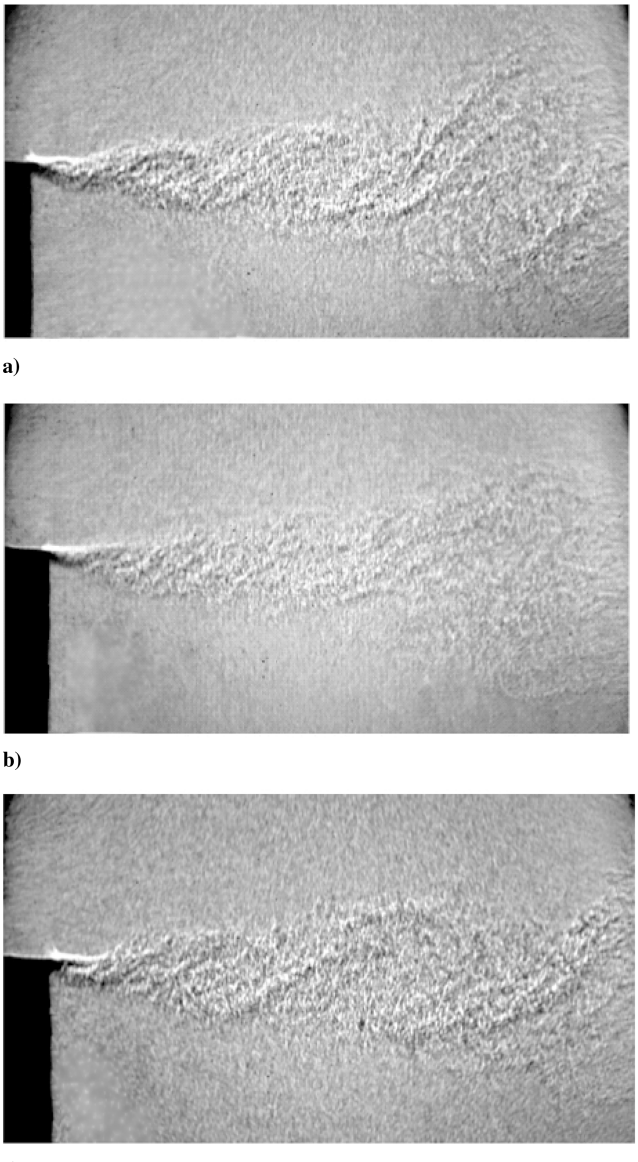

**a)**

**b)**

**c)**

**Fig. 7 Examples of shadowgraph images of the shear layer for a) unforced case, b) with forcing at $St = 0.016$, which corresponded to an ensemble-average 27.5% decrease in $\mathrm{OPD_{rms}}$, and c) with forcing at $St = 0.03$, which corresponded to an ensemble-average 16.9% increase in $\mathrm{OPD_{rms}}$; b–c) shadowgraphs show visual evidence of LSS and LSR separated shear layer control, respectively.**

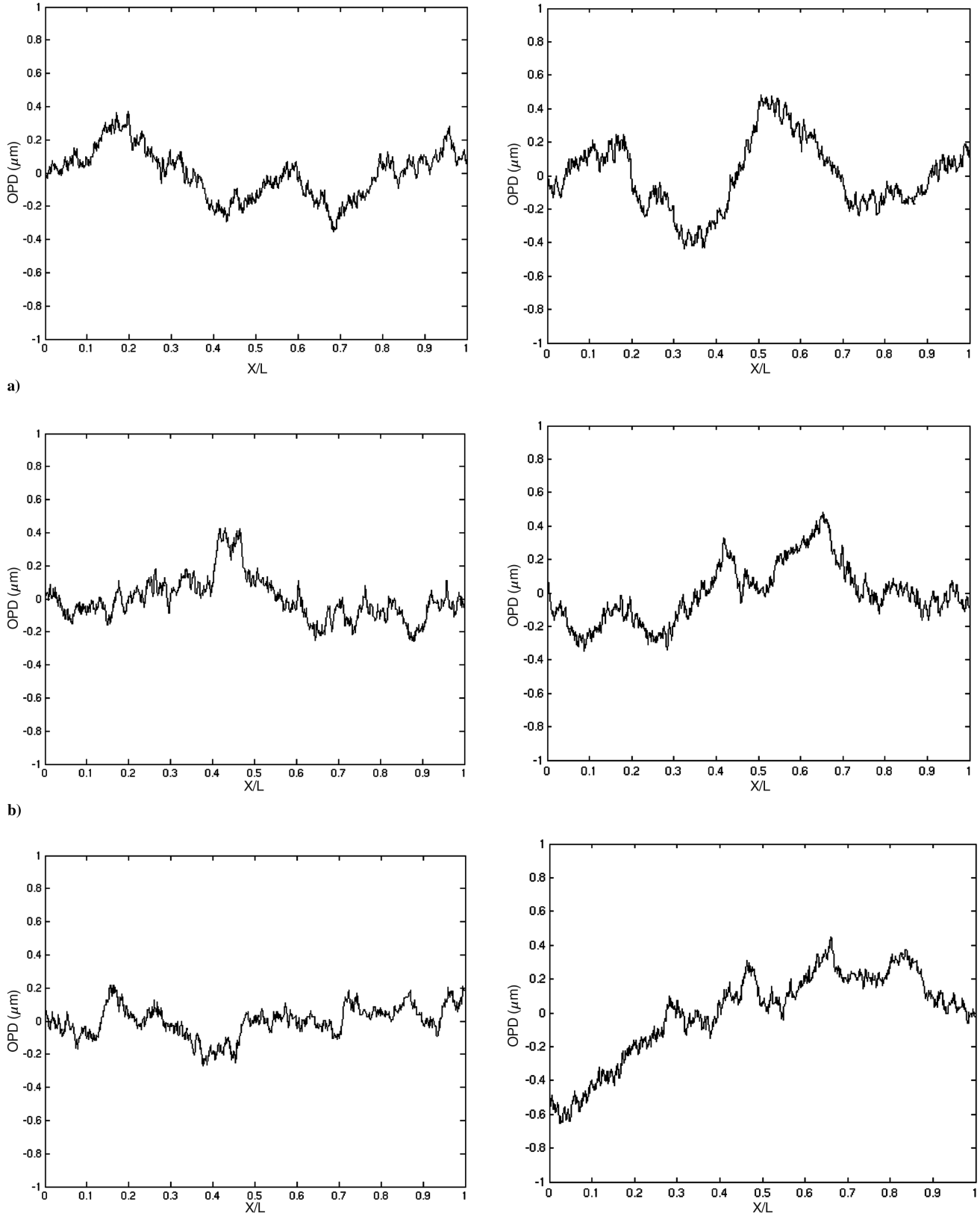


**Fig. 8 Examples of OPD profiles that resulted from laser propagation through a turbulent compressible shear layer with the following Strouhal numbers based on the plasma pulsing frequency and momentum thickness: a) unforced, $St = 0.003$; b) $St = 0.016$ and $St = 0.03$; c) $St = 0.042$ and $St = 0.083$.**

turbulence-aberrated refractive index fields, which correspond to the density fields within the shear layer, have been found to demonstrate a $k^{-5/3}$ power law scaling. By inspection, it can be seen that the forced shear layers, which resulted in significantly lower $\mathrm{OPD}_{\mathrm{rms}}$ values, have corresponding spectra with fewer total distribution in the low wave number region, which refers to the first decade of frequencies. Because this region is where the distribution of large-scale structures would be present due to high aero-optical aberrations,

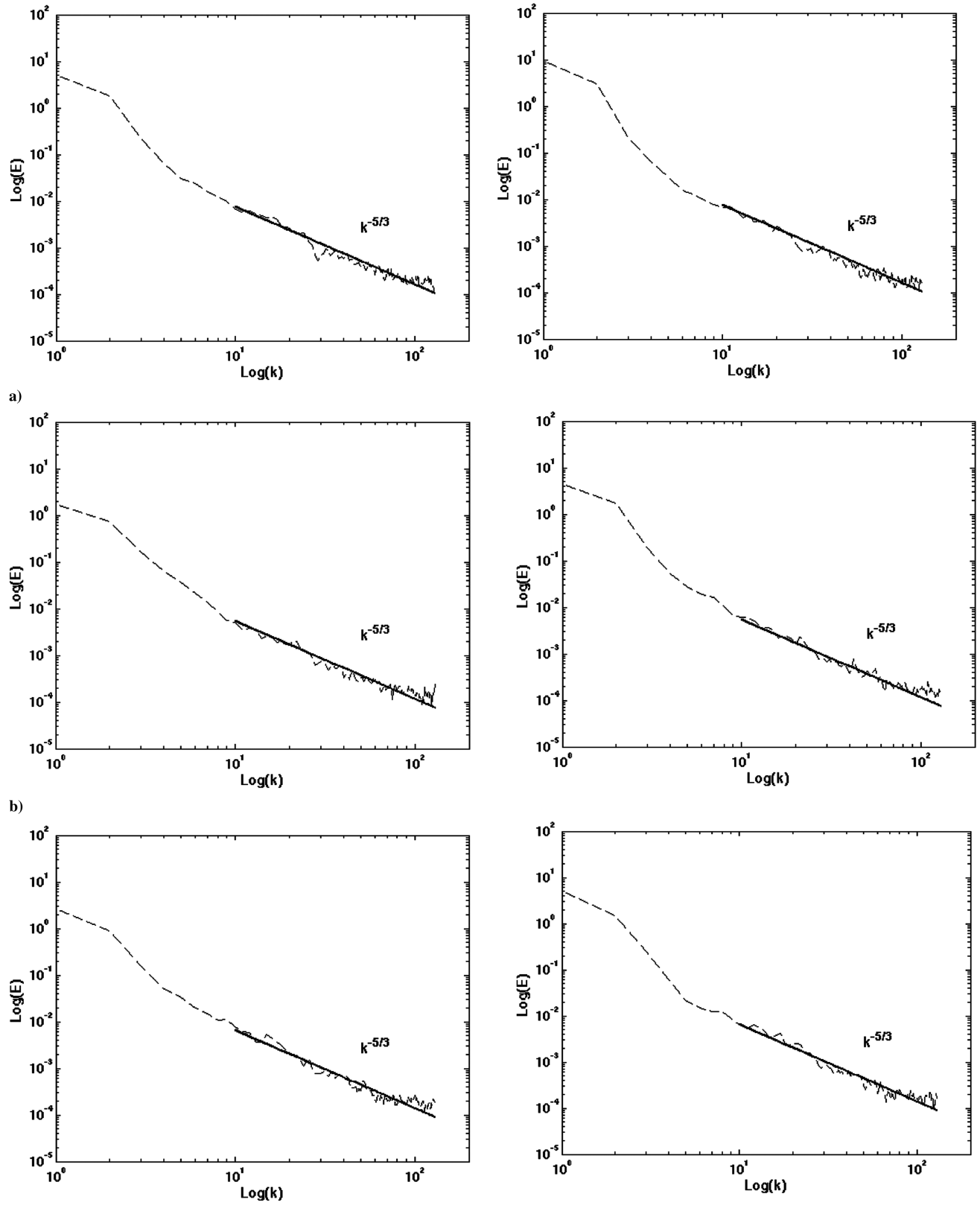


**Fig. 9 Power spectra calculated from OPD profiles shown in Fig. 8 with the following Strouhal numbers; a) unforced and $St = 0.003$; b) $St = 0.016$ and $St = 0.03$; c) $St = 0.042$ and $St = 0.083$. Each figure represents the average power spectra calculated from 10 individual OPD profiles. The calculations were made with 129 point frequencies.**

reductions compared with the spectra of the unforced shear layer further suggest that the interaction between the turbulent separated shear layer and the PPA have resulted in direct reductions in aero-optical aberrations based on direct large structure suppression.

Figure 10 shows the percent change in the $OPD_{rms}$ compared with the unforced case plotted against the Strouhal number for each pulsing frequency tested. Figure 11 shows the average power spectrum for the OPD profiles that correspond to the unforced shear

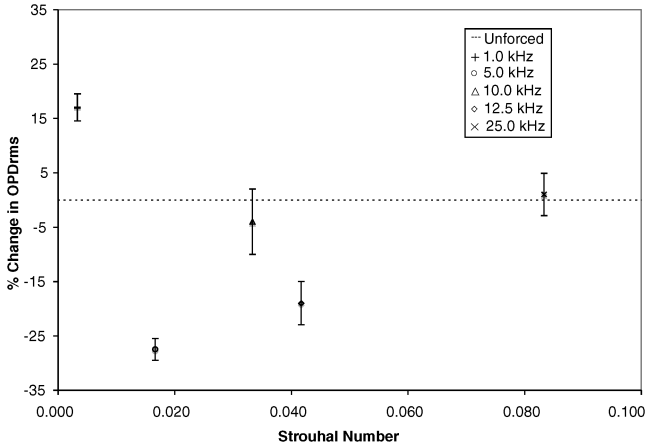


**Fig. 10 Resulting values of the percent change in $OPD_{rms}$ for various plasma pulsing frequencies compared with the unforced case with an $OPD_{rms}$ value of 0.2 $\mu$m. Plasma was generated at 50.0 kHz for each case.**

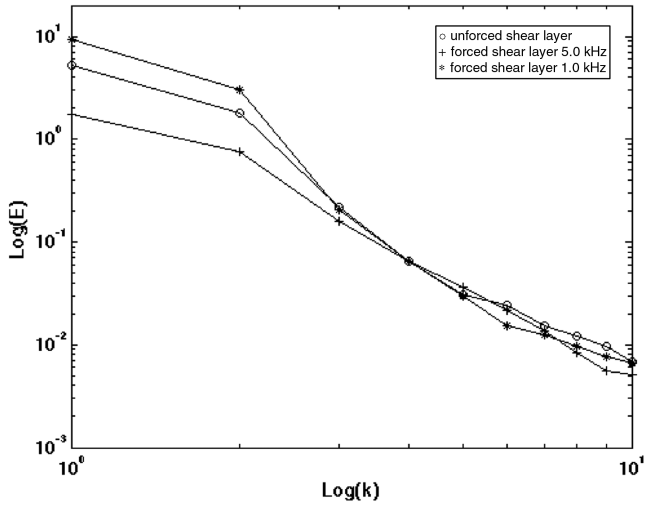


**Fig. 11 Superimposed power spectra results for the first decade of wave numbers.**

layer, as well as the forced shear layer that resulted in the highest levels of LSS and LSR. Each of the results shown in these two figures represent average results for ten individual experiments. Figure 11, in particular, allows for direct comparison of the power spectra in the low wave number region, further confirming that the suppression vs regularization of large organized turbulent structures, as evidenced by the LSS and LSR cases shown, is associated with reduction vs increase of energy at the lowest wave numbers relative to the unforced case, respectively.

## VI. Conclusions

Aero-optical aberrations incurred by an optical wave front propagating through a compressible separated turbulent separated shear flow have been examined in relation to their reduction as caused by the suppression of large turbulent structure formation within the shear layer. Frequency forcing of the shear layer was accomplished through the implementation of a pulsed plasma actuator, which induces a body force on the flow near the point of separation. The levels of direct reduction in the aero-optical aberrations were determined by analyzing the optical path difference root mean square of the turbulence-aberrated optical wave front profiles for the unforced shear layer compared with the forced shear layer at varying pulsing frequencies. Preliminary results suggest that the PPA can be used to achieve direct reductions in aero-optical aberrations of up to 27.5%, which was achieved by generating plasma at 50.0 kHz and pulsing it at 5.0 kHz with a duty cycle of 30%. These direct reductions in aero-optical aberrations correspond to suppression of the large-scale organization within the turbulent shear layer.

By analyzing the spectra of the various OPD profiles, it was found that the plasma forcing did not adversely affect the inertial ranges of scales within the refractive turbulence fields, as profiled by the Shack–Hartmann sensor. The low wave numbers, which correspond to large aero-optical aberrations and therefore large turbulent structures, were found to be less frequent in the spectra corresponding to the cases with plasma pulsed at 5.0 and 12.5 kHz. This reduction in large aero-optical aberrations, as seen by the spectra results, agrees with the reduced values of the $OPD_{rms}$ for the experimental data with the same pulsing frequency. Additionally, the shadowgraphs shown in Fig. 7 further suggest that the decreases and increases in the overall laser aberrations are the result of LSS and LSR flow control, respectively. Although these results do not directly reveal the full mechanisms of LSS and LSR, they show the effectiveness of plasma control for reducing the laser aberrations with LSS. Additionally, the results are consistent with other research related to LSS [17].

## Acknowledgments

We express special thanks to Philip Garcia and Jennifer Nathman, whose preliminary efforts on the Shack–Hartmann wave front sensor and the pulsed plasma actuator, respectively, made this research possible, as well as to Fazlul Zubair and Jennifer Shockro for assistance with the experiments. We are also thankful to D. Dunn-Rankin, S. Elghobashi, E. Jumper, R. Liebeck, and M. Samimy for useful discussions. We are especially grateful to the referees for their perceptive and insightful comments.

## References

[1] Liepmann, H. W., "Deflection and Diffusion of a Light Ray Passing Through a Boundary Layer," Douglas Aircraft Rept. SM-14397, May 1952.

[2] Kyrazis, D., "Optical Degradation by Turbulent Free Shear Layers," *Optical Diagnostics in Fluid and Thermal Flow*, edited by S. S. Cha, and J. D. Trolinger, Society of Photo-Optical Instrumentation Engineers, Orlando, FL, 1993, pp. 170–181.

[3] Jumper, E. J., and Fitzgerald, E. J., "Recent Advances in Aero-Optics," *Progress in Aerospace Sciences*, Vol. 37, No. 3, 2001, pp. 299–339. doi:10.1016/S0376-0421(01)00008-2

[4] Pope, S. B., *Turbulent Flows*, Cambridge Univ. Press, Cambridge, England, U.K., 2000.

[5] Catrakis, H. J., Aguirre, R. C., Nathman, J. C., and Garcia, P. J., "Large Scale Refractive Turbulent Interfaces and Aero-Optical Interactions in High Reynolds Number Compressible Separated Shear Layers," *Journal of Turbulence*, Vol. 7, No. 54, 2006, pp. 1–21. doi:10.1080/14685240600800069

[6] Dimotakis, P. E., Catrakis, H. J., and Fourguette, D. C. L., "Flow Structure and Optical Beam Propagation in High-Reynolds-Number Gas-Phase Shear Layers and Jets," *Journal of Fluid Mechanics*, Vol. 433, June 2001, pp. 105–134.

[7] Jones, M., and Bender, E. E., "CFD-Based Computer Simulation of Optical Turbulence Through Aircraft Flowfields and Wakes," *AIAA 32rd Plasmadynamics and Lasers Conference*, AIAA Paper 2001-2798, June 2001.

[8] Catrakis, H. J., and Aguirre, R. C., "New Interfacial Fluid Thickness Approach in Aero-Optics with Applications to Compressible Turbulence," *AIAA Journal*, Vol. 42, No. 10, 2004, pp. 1973–1981. doi:10.2514/1.547

[9] Catrakis, H. J., Aguirre, R. C., and Nathman, J. C., "Large-Reynolds-Number Turbulent Fluid Interfaces and the Upper Range of Scales," *AIAA 42nd Aerospace Sciences Meeting and Exhibit*, AIAA Paper 2004-1113, 2004.

[10] Vukasinovic, B., and Glezer, A., "Transitory Fluidic Control of Turbulent Shear Flows," *AIAA 36th Fluid Dynamics Conference and Exhibit*, AIAA 2006-3227, June 2006.

[11] Wiltse, J. M. and Glezer, A., "Direct Excitation of Small-Scale Motions in Free-Shear Flows," *Physics of Fluids*, Vol. 10, No. 8, 1998, pp. 2026–2036. doi:10.1063/1.869718

[12] MacKinnon, C. G., and Koochesfahani, M. M., "Flow Structure and

Mixing in a Low Reynolds Number Forced Wake Inside a Confined Channel," *Physics of Fluids*, Vol. 9, No. 10, 1997, pp. 3099–3101. doi:10.1063/1.869418

[13] Tsai, Y.-P., and Christiansen, W. H., "Two-Dimensional Numerical Simulation of Shear Layer Optics," *AIAA Journal*, Vol. 28, No. 12, 1990, p. 2092. doi:10.2514/3.10526

[14] Chew, L., and Christiansen, W., "Coherent Structure Effects on Optical Performance of Plane Shear Layers," *AIAA Journal*, Vol. 29, No. 1, 1991, pp. 76–80. doi:10.2514/3.10547

[15] Chew, L., and Christiansen, W., "Experimental Investigation of Transitional Free Shear Layer Optics," *AIAA Journal*, Vol. 31, No. 12, 1993, pp. 2290–2295. doi:10.2514/3.11927

[16] Zubair, F. R., and Catrakis, H. J., "Aero-Optical Interactions Along Laser Beam Propagation Paths in Compressible Turbulence," *AIAA Journal*, Vol. 45, No. 7, 2007, pp. 1663–1674. doi:10.2514/1.27342

[17] Stanek, M., Raman, G., Ross, J. A., Odedra, J., Peto, J., Alvi, F., and Kibens, V., "High Frequency Acoustic Suppression. The Role of Mass Flow, the Notion of Superposition, and the Role of Inviscid Instability: A New Model (Part 2)," *AIAA 8th Aeroacoustics Conference and Exhibit*, AIAA Paper 2002-2404, June 2002.

[18] Siegenthaler, J. P., Jumper, E. J., and Asghar, A., "Preliminary Study in Regularizing the Coherent Structures in a Planar, Weakly-Compressible, Free Shear Layer," *AIAA 41st Aerospace Sciences Meeting and Exhibit*, AIAA Paper 2003-0680, Jan. 2003.

[19] McMackin, L., Masson, B., Clark, N., Pierson, R. E., and Chen, E., "Hartmann Wave Front Sensor Studies of Dynamic Organized Structures in Flowfields," *AIAA Journal*, Vol. 33, No. 11, 1995, pp. 2158–2164. doi:10.2514/3.12961

[20] Neal, D. R., O'Hern, T. J., Torczynski, J. R., Warren, M. E., Shul, R., and McKechnie, T. S., "Wavefront Sensors for Optical Diagnostics in Fluid Mechanics: Application to Heated Flow, Turbulence, and Droplet Evaporation," *Proceedings of SPIE: The International Society for Optical Engineering*, Vol. 2005, 1993, pp. 194–203. doi:10.1117/12.163703

[21] Garcia, P., "Laser Wavefront Propagation in Turbulence and High-Resolution Shack–Hartmann Sensing," M.S. Thesis, Univ. of California, Irvine, CA, 2006.

[22] Aguirre, R., "Turbulent Fluid Interfaces with Applications to Mixing and Aero-Optics," Ph.D. Thesis, Univ. of California, Irvine, CA, 2005.

[23] Nathman, J., "Initial Study of Flow Control on a Single Stream Separated Shear Layer Using a Plasma Actuator," M.S. Thesis, Univ. of California, Irvine, CA, 2005.

[24] Oster, D., and Wygnanski, I., "Forced Mixing Layer Between Parallel Streams," *Journal of Fluid Mechanics*, Vol. 123, Oct. 1982, pp. 91–130. doi:10.1017/S0022112082002973

[25] Ho, C.-M., and Huerre, P., "Perturbed Free Shear Layers," *Annual Review of Fluid Mechanics*, Vol. 16, Jan. 1984, pp. 365–424. doi:10.1146/annurev.fl.16.010184.002053

[26] McLaughlin, T., Munska, M., Vaeth, J., Dauwalter, D., Goode, J., and Siegal, S., "Plasma-Based Actuators for Cylinder Wake Vortex Control," *AIAA 2nd Flow Control Meeting*, AIAA Paper 2004-2129, 2004.

[27] Corke, T. C., Post, M. L., and Orlov, D. M., "SDBD Plasma Enhanced Aerodynamics: Concepts, Optimization and Applications," *Progress in Aerospace Sciences*, Vol. 43, Nos. 7–8, 2007, pp. 193–217. doi:10.1016/j.paerosci.2007.06.001

[28] Post, M., and Corke, T., "Separation Control Using Plasma Actuators: Dynamic Stall Control on an Oscillating Airfoil," *AIAA 2nd Flow Control Meeting*, AIAA 2004-2517, June 2004.

[29] Jacob, J. D., Ramakumar, K., Anthony, R., and Rivir, R. B., "Control of Laminar and Turbulent Shear Flows Using Plasma Actuators," *4th International Symposium on Turbulence and Shear Flow Phenomenon*, Paper TSFP4-225, June 2005.

[30] Porter, C., McLaughlin, T., Enloe, C., Font, G., Roney, J., and Baughn, J., "Boundary Layer Control Using a DBD Plasma Actuator," *Collection of Technical Papers: 45th AIAA Aerospace Sciences Meeting*, Vol. 14, AIAA, Reston, VA, 2007, pp. 9630–9643.

J. Gore
*Associate Editor*